

# Mössbauer spectroscopy— an indispensable tool in solid state research\*

Philipp Gülich,<sup>a</sup> Christian Schröder<sup>b,c</sup> and Volker Schünemann<sup>d</sup>

<sup>a</sup>Institut für Anorganische Chemie und Analytische Chemie, Johannes Gutenberg-Universität, Staudinger Weg 9, 55128 Mainz, Germany. E-mail: guetlich@uni-mainz.de

<sup>b</sup>Lehrstuhl für Hydrologie, Universität Bayreuth, Universitätsstraße 30, 95447 Bayreuth, Germany

<sup>c</sup>Zentrum für Angewandte Geowissenschaften, Eberhard Karls Universität, Sigwartstr. 10, 72076 Tübingen, Germany. E-mail: christian.schroeder@ifg.uni-tuebingen.de

<sup>d</sup>Fachbereich Physik, Technische Universität Kaiserslautern, Erwin-Schrödinger-Str. 56, D-67663 Kaiserslautern, Germany. E-mail: schuene@physik.uni-kl.de

## Introduction

More than 50 years ago, the German physicist Rudolf L. Mössbauer, whilst working on his doctoral thesis under Professor Maier-Leibnitz at the Technical University in Munich and at the Max-Planck Institute in Heidelberg, discovered the *recoilless nuclear resonance absorption of gamma rays* which became known as the Mössbauer Effect.<sup>1–3</sup> He was awarded the Nobel Prize for Physics in 1961 as one of the youngest recipients of this most prestigious award. The phenomenon rapidly developed to a new spectroscopic technique, which now bears Rudolf Mössbauer's name. Mössbauer spectroscopy has made valuable contributions to widespread applications in solid state research, from fundamental studies in physics, chemistry, metallurgy, biological- and geo-sciences as well as to industrial and materials science applications. Figure 1 gives an overview of applications of Mössbauer spectroscopy in various research disciplines.

Mössbauer spectroscopy has become an elegant tool for the study of electronic

structure, bonding properties, molecular symmetry, magnetic behaviour and phase transitions in the solid state, which forms the basis for identifying all kinds of materials. Mössbauer spectroscopy allows for non-destructive phase analysis, which is often employed routinely as a "fingerprint" method. Even substances that *a priori* do not contain a Mössbauer-active nuclide have been extensively studied by doping the sample with small amounts of a Mössbauer probe nuclide

(for example, <sup>57</sup>Fe). Also, although the Mössbauer effect is observable only in solid material, this does not necessarily have to be in a well-crystallised shape; it is well established that Mössbauer spectra may even be recorded of frozen solutions.

Not only has the applicability of Mössbauer spectroscopy enormously spread in the characterisation of materials in the broadest sense, from fundamental research to practical industrial

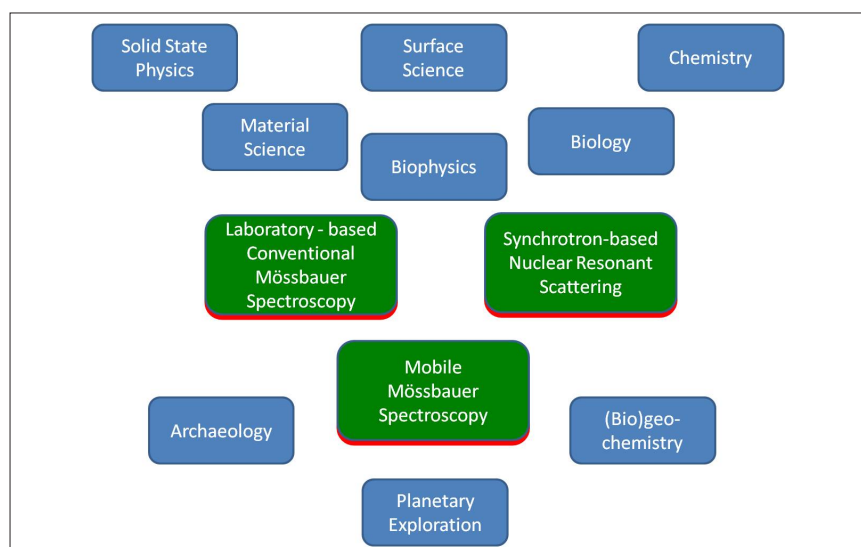


Figure 1. Overview of the applications and impact of Mössbauer spectroscopy.

\*In memoriam Professor Rudolf Ludwig Mössbauer

Mössbauer Periodic Table

1																	18	
H																		He
Li	Be											B	C	N	O	F	Ne	
Na	Mg	3	4	5	6	7	8	9	10	11	12	Al	Si	P	S	Cl	Ar	
K <sup>1</sup>	Ca	Sc	Ti	V	Cr	Mn	Fe <sup>2</sup>	Co	Ni <sup>1</sup>	Cu	Zn <sup>1</sup>	Ga	Ge <sup>2</sup>	As	Se	Br	Kr <sup>1</sup>	
Rb	Sr	Y	Zr	Nb	Mo	Tc <sup>1</sup>	Ru <sup>2</sup>	Rh	Pd	Ag	Cd	In	Sn <sup>2</sup>	Sb <sup>1</sup>	Te <sup>1</sup>	I <sup>2</sup>	Xe <sup>2</sup>	
Cs <sup>1</sup>	Ba <sup>1</sup>	La <sup>1</sup>	Hf <sup>4</sup>	Ta <sup>2</sup>	W <sup>7</sup>	Re <sup>1</sup>	Os <sup>6</sup>	Ir <sup>4</sup>	Pt <sup>2</sup>	Au <sup>1</sup>	Hg <sup>1</sup>	Tl	Pb	Bi	Po	At	Rn	
Fr	Ra	Ac																
			Ce	Pr <sup>1</sup>	Nd <sup>2</sup>	Pm <sup>1</sup>	Sm <sup>6</sup>	Eu <sup>4</sup>	Gd <sup>9</sup>	Tb <sup>1</sup>	Dy <sup>6</sup>	Ho <sup>1</sup>	Er <sup>5</sup>	Tm <sup>1</sup>	Yb <sup>6</sup>	Lu <sup>1</sup>		
			Th <sup>1</sup>	Pa <sup>1</sup>	U <sup>3</sup>	Np <sup>1</sup>	Pu <sup>1</sup>	Am <sup>1</sup>	Cm	Bk	Cf	Es	Fm	Md	No	Lw		

**Figure 2.** Periodic table of the elements; those in which the Mössbauer effect has been observed are marked appropriately. (Reproduced from the 1974 Edition of Reference 9 with permission.)

applications, remarkable progress has also taken place in instrumentation and methodology. Most spectacular, for instance, is the miniaturisation of a laboratory spectrometer by scaling down by a factor of *ca* 100 to a device, known as MIMOS (Miniaturised Mössbauer Spectrometer),<sup>4</sup> which has been operating on the surface of the planet Mars as well as in many mobile analytical studies on Earth; examples will be described below. Another most remarkable development began in the mid 1980s, with the experimental proof by Gerda *et al.*<sup>5</sup> that nuclear resonance fluorescence is also possible with synchrotron radiation instead of a radioactive source. Two methods have emerged thereof: nuclear forward scattering (NFS) for the measurement of hyperfine interaction and nuclear inelastic scattering (NIS) of synchrotron radiation for the measurement of phonon spectra of local vibrational modes near to the Mössbauer probe nucleus. Recent work employing these techniques will be discussed below.

Many textbooks and review articles on principles, experimental aspects and applications of Mössbauer spectroscopy have appeared. We refer to only a few of them which, in our opinion, seem to be recommendable for further reading and learning in more detail about this spectroscopic technique.<sup>6–8</sup>

## Background

The Mössbauer effect has been detected for a total of nearly 90  $\gamma$ -ray transitions in 72 isotopes of 42 different elements. Figure 2 shows the Periodic Table of the elements in which the Mössbauer-active elements are marked. Due to several criteria (suitable lifetime of nuclear excited state, transition energy, easy accessibility and handling) only *ca* 20 elements can be studied by Mössbauer spectroscopy, for example, iron, tin, antimony, tellurium, iodine, gold, nickel, ruthenium, iridium, tungsten, krypton, xenon, many of the rare earth elements and neptunium. The most prominent “Mössbauer nuclide” is <sup>57</sup>Fe. More than 90% of the nearly 80,000 publications that have appeared so far refer to <sup>57</sup>Fe spectroscopy.

## Mössbauer effect

The Mössbauer effect is the *recoilless nuclear resonance absorption and emission of  $\gamma$ -rays*, similar to the acoustic resonance between two tuning forks with the same frequency  $f_s = f_r$  for sender (s) and receiver (r). A nucleus with *Z* protons and *N* neutrons in an excited state of energy  $E_e$  and mean lifetime  $\tau$  of typically 100 ns undergoes transition to the ground state of energy  $E_g$  by emitting a  $\gamma$ -quantum of energy  $E_\gamma = E_e - E_g$ . The  $\gamma$ -quantum may be absorbed by a nucleus of the same kind (same *Z* and *N*) in its ground state, whereby transi-

tion to the excited state of energy  $E_e$  takes place (resonance absorption). The subsequent transition to the ground state emits again a  $\gamma$ -quantum (resonance fluorescence) or a conversion electron  $e^-$  (with nearly ten times higher probability than  $\gamma$ -emission). The mean lifetime  $\tau$  determines the width,  $\Gamma$ , of the resonance lines by  $\Gamma \cdot \tau = \hbar$  ( $\hbar = h/2\pi$  which is Planck's constant).

Resonance absorption is observable only if the emission and absorption lines overlap sufficiently. By emission or absorption of  $\gamma$ -quanta with energy  $E_\gamma$  in a freely moving atom or molecule (gas, liquid), the atom (molecule) of mass *m* suffers a recoil effect with energy  $E_R = E_\gamma^2/2mc^2$ , which is several orders of magnitude larger than the natural line width  $\Gamma$ . No resonance is possible between free atoms or molecules. The Mössbauer effect cannot, therefore, be observed for freely moving atoms or molecules, i.e. in gaseous or liquid state. In the solid state, recoilless emission and absorption of  $\gamma$  quanta is possible, and the essentially unshifted transition lines can (at least partially) overlap and nuclear resonance absorption can be observed. This was experimentally proven by Rudolf Mössbauer by cooling the source and absorber down to temperatures near to that of liquid nitrogen, where atoms are tightly bound in the lattice and the recoil effect is considerably suppressed. Mössbauer was able to rationalise this phenomenon on quantum-mechanical grounds and showed that, for a certain probability, which is relatively high for hard and low for a soft material, atoms as lattice harmonic oscillators do not change their quantum-mechanical state upon emission or absorption of  $\gamma$ -quanta (*zero-phonon processes*).<sup>1–3</sup> Only for this fraction, known as the *Lamb–Mössbauer fraction*, can nuclear resonance absorption of  $\gamma$ -rays (Mössbauer effect) be observed. The main components of a modern Mössbauer spectrometer and its operational use are described in detail elsewhere.<sup>8</sup>

## Hyperfine interactions and Mössbauer parameters

Three kinds of hyperfine interactions may be observed in a Mössbauer spectrum:

1. *Electric monopole interaction* is the Coulomb interaction between protons of the nucleus and electrons (mainly s-electrons) penetrating the nuclear field. The observable Mössbauer parameter is the *isomer shift*  $\delta$ . Isomer shift values give information on the oxidation state, spin state and bonding properties such as covalency and electronegativity.

2. *Electric quadrupole interaction* between the nuclear quadrupole moment of the ground and/or excited state and an inhomogeneous electric field at the nucleus. The observable Mössbauer parameter is the *quadrupole splitting*  $\Delta E_Q$ . The information derived from the quadrupole splitting refers to oxidation state, spin state and site symmetry determined by electronic structure and nearby lattice surroundings.

3. *Magnetic dipole interaction* between the nuclear magnetic dipole moment and a magnetic field. The observable Mössbauer parameter is the *magnetic splitting*  $\Delta E_M$ . This quantity gives information on the magnetic properties of the material under study.

*Electric monopole (Coulombic) interaction* shifts the nuclear energy levels of ground and excited states, but does not split degenerate sublevels of different magnetic spin quantum numbers. If

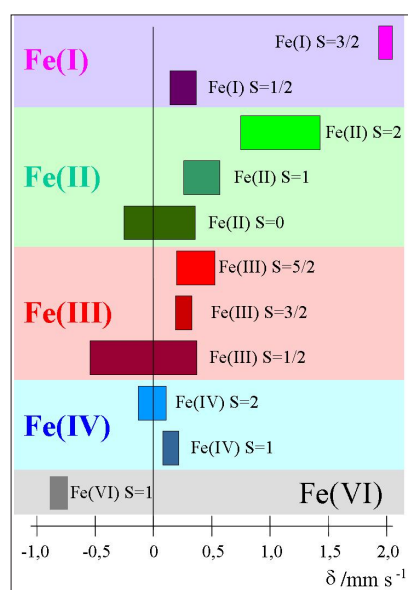


**Figure 3.** Ranges of isomer shift values expected for different oxidation and spin states of iron compounds (reproduced from Reference 17 with permission).

the source and absorber materials are different, which is generally the case in a Mössbauer experiment, the s-electron densities at the nuclei of source and absorber are different, which causes different energy shifts of the nuclear levels. Thus the transition energies  $E_S$ ,  $E_A$  in the source and absorber, respectively, are different. The difference is denoted as *Isomer shift*  $\delta = E_A - E_S$ . It can be measured by bringing the emission and absorption lines to overlap, i.e. to resonance, by making use of the Doppler effect, whereby source and absorber are moved relative to each other at variable velocities. The isomer shift,  $\delta$ , appears in the spectrum as the difference between the position of the resonance signal and zero Doppler velocity, or between the barycentre of an electromagnetically split spectrum and zero velocity. As an example, Figure 3 shows isomer shift values (from <sup>57</sup>Fe measurements) expected for different oxidation and spin states of iron compounds.

*Electric quadrupole interaction* occurs if at least one of the nuclear states involved possesses an electric quadrupole moment (which is the case for nuclear states with spin  $I > 1/2$ ) and if the electric field at the nucleus is inhomogeneous. In the case of <sup>57</sup>Fe the first excited state (14.4 keV state) has spin  $I = 3/2$  and, therefore, also an electric quadrupole moment. If the electric field at the nucleus is inhomogeneous due to non-cubic valence electron distribution and/or non-cubic lattice surroundings, electric quadrupole interaction sets in and splits the degenerate  $I = 3/2$  level into two substates with magnetic spin quantum numbers  $m_I = \pm 3/2$  and  $\pm 1/2$  (see Figure 4). Three examples are shown in Figure 5. The upper spectrum of the high spin compound  $[\text{Fe}(\text{H}_2\text{O})_6]^{2+}\text{SO}_4 \cdot \text{H}_2\text{O}$  with spin  $S = 2$  exhibits a rather large quadrupole splitting due to non-cubic distribution of the six valence electrons of the  $\text{Fe}^{2+}$  ion over the five d-orbitals which are split due to Jahn–Teller distortion such that the lowest orbital carries two electrons, whereas the other four orbitals are only singly occupied. The spectrum of the low spin complex compound of  $\text{K}_4[\text{Fe}(\text{CN})_6]$  with  $S = 0$  shown in the

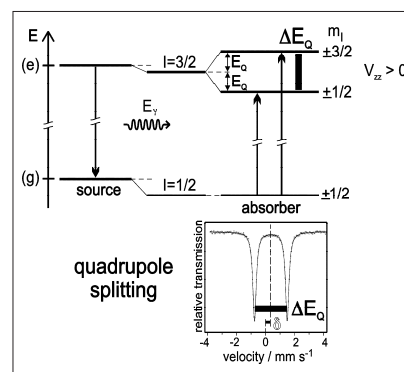


**Figure 4.** Quadrupole splitting of the excited state of <sup>57</sup>Fe with  $I = 3/2$  and the resulting Mössbauer spectrum (schematic). Quadrupole interaction splits the spin quartet into two degenerate sublevels  $|I, \pm m_I\rangle$  with energy separation  $\Delta E_Q = 2E_Q$ . The ground state with  $I = 1/2$  remains unsplit. The nuclear states are additionally shifted by electric monopole interaction giving rise to the isomer shift  $\delta$  (adapted with permission from Reference 8).

middle of Figure 5 exhibits no quadrupole splitting, because the six CN ligands sit in the corner of a regular octahedron (cubic symmetry) and the six valence electrons are also arranged in cubic symmetry. If, however, one of the six CN ligands is replaced by a different ligand, dramatic deviation from cubic symmetry occurs resulting in the observed quadrupole splitting as shown in Figure 5 (lower part) for the low-spin complex compound  $\text{Na}_2[\text{Fe}(\text{CN})_5\text{NO}]$ . *Magnetic dipole splitting* occurs if the Mössbauer probe nuclide “feels” a sufficiently strong magnetic field. This can be created intrinsically by the substance under investigation through various mechanisms<sup>8</sup> or simply by applying an external magnetic field. Magnetic dipole interaction leads to splitting of nuclear states with  $I > 1/2$  into  $2I + 1$  substates differing in size and sign of the magnetic nuclear spin quantum numbers  $m_I$ . In the case of <sup>57</sup>Fe magnetic dipole interaction leads to four substates of the excited state ( $I = 3/2$ ) and two of the ground nuclear state ( $I = 1/2$ ). According to certain selection rules ( $\Delta I = \pm 1$ ,  $\Delta m_I = 0, \pm 1$ ) six transition lines are allowed and the resulting Mössbauer spectrum shows a magnetically split sextet, with equal distances between

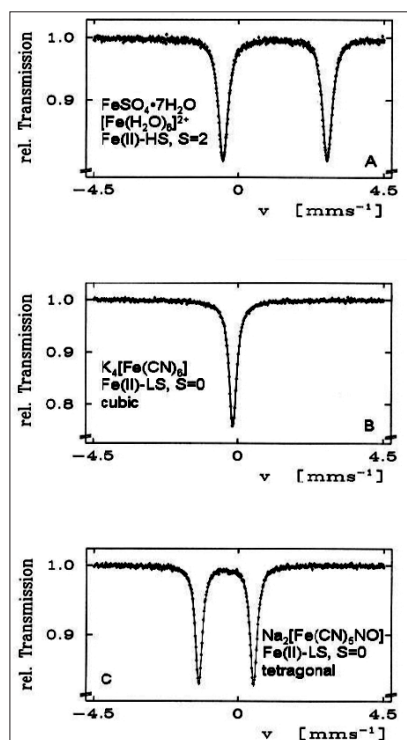


**Figure 5.**  $^{57}\text{Fe}$  Mössbauer spectra of three selected Fe(II) compounds. The occurrence of quadrupole splitting in compounds A and C and the absence of it in compound B is discussed in the text (reproduced from Reference 17 with permission).

the six resonance peaks (see Figure 6). Often, electric quadrupole and magnetic

dipole interaction occur simultaneously in a substance. In this case the six peaks are no longer equidistant due to distortion by electric quadrupole interaction in the presence of a relatively strong magnetic field.

### Selected applications

Mössbauer spectroscopy has developed into an elegant and versatile analytical instrument in solid state research. In routine analyses it can give a quick answer on the valence state (oxidation state, spin state), local symmetry or magnetic properties of a Mössbauer atom contained in the material of interest. It has also proved invaluable in studying various kinds of phase transitions, even in cases where the material does not contain a Mössbauer-active nuclide as constituent it can be doped with one in small concentrations. Often, Mössbauer spectroscopy turns out to be the only technique for special investigations and information. Whereas conventional Mössbauer spectroscopy, often employed as a “fingerprint method”, has been firmly established within the realm of other techniques for solid state research, advanced instrumental developments such as the miniaturisation of the laboratory spectrometer and

the use of synchrotron radiation instead of radioactive nuclides as sources have opened new pathways and provide the means for studies of special problems. Selected examples using various facets of Mössbauer spectroscopy will be described below.

### Applications of conventional Mössbauer spectroscopy

**Study of thermal- and light-induced spin state switching in iron compounds.** Thermally-induced spin transition from a high spin (HS) state with maximum unpaired electrons to a low spin (LS) state with minimum unpaired electrons, also known as spin crossover (SCO), can be encountered with many Fe(II) and Fe(III) compounds, if the energy difference between the two spin states becomes comparable to the spin pairing energy.<sup>10,11</sup>  $^{57}\text{Fe}$  Mössbauer spectroscopy is ideally suited to follow quantitatively the spin transition as a function of temperature, since the individual spectra of the HS and LS states are entirely different and well resolved in most cases. An example is shown in Figure 7.  $[\text{Fe}^{\text{II}}(\text{phen})_3]\text{X}_2$  (phen = 1.10-phenanthroline) is a low spin compound at all temperatures under study as confirmed by the characteristic Mössbauer spectra on the

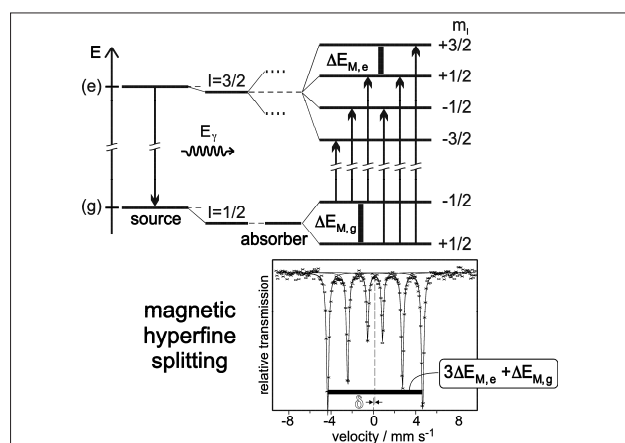


**Figure 6.** Magnetic dipole splitting (nuclear Zeeman effect) in  $^{57}\text{Fe}$  and resultant Mössbauer spectrum (schematic). The mean energy of the nuclear states is shifted by electric monopole interaction which gives rise to additional isomer shift  $\delta$ .  $\Delta E_{M,g} = g_{\mu N} B$  and  $\Delta E_{M,e} = g_{\mu N} B$  refer to the Zeeman energies of the ground and the excited states, respectively. The splitting of the  $l=3/2$  state into two dotted lines in the middle panel indicates the effect of quadrupole splitting discussed before (reproduced from Reference 8 with permission).

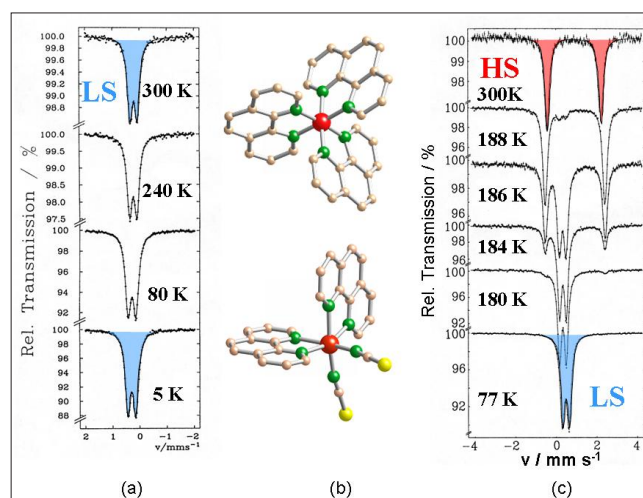


**Figure 7.** (a) Mössbauer spectra of  $[\text{Fe}(\text{phen})_3]\text{X}_2$  recorded over the temperature range 300–5 K. (b) View of the crystal structures of  $[\text{Fe}(\text{phen})_3]^{2+}$  (top) and  $[\text{Fe}(\text{phen})_2(\text{NCS})_2]$  (bottom). (c) Mössbauer spectra of  $[\text{Fe}(\text{phen})_2(\text{NCS})_2]$  recorded over the temperature range 300–77 K reflecting the thermally induced HS  $\leftrightarrow$  LS spin transition<sup>11,12</sup> (reproduced from Reference 17 with permission).

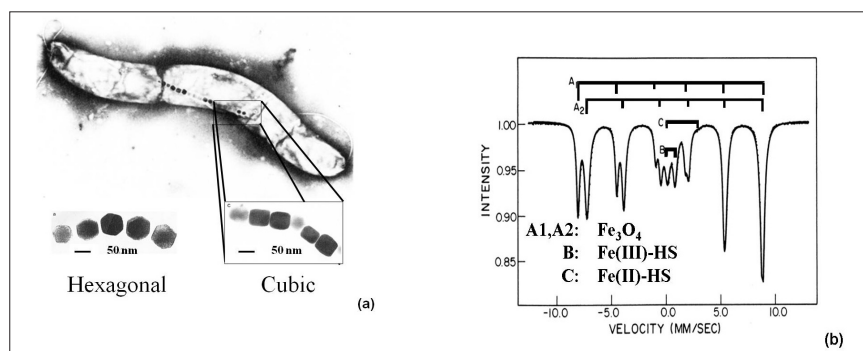


**Figure 8.** (a) Hexagonal- and cubic-shaped  $\text{Fe}_3\text{O}_4$  nanoparticles identified in the magnetotactic bacteria *Aquaspirillum magnetotacticum*. (b)  $^{57}\text{Fe}$  Mössbauer spectrum of magnetic particles extracted from the same bacteria and recorded at 200K.<sup>13</sup> The main component ( $A_1$ ,  $A_2$ ) refers to magnetite,  $\text{Fe}_3\text{O}_4$ , which serves as a geomagnetic compass and enables the bacteria to follow the earth's magnetic field (reproduced from Reference 13 with permission).

left of Figure 7. If one of the relatively strong phen ligands, which occupies two coordination positions of the octahedron, is replaced by two mono-functional  $\text{NCS}^-$  groups, the average ligand field strength becomes weaker and the compound  $[\text{Fe}^{\text{II}}(\text{phen})_2(\text{NCS})_2]$  adopts a high spin character at room temperature. The Mössbauer spectrum at 300 K shows the typical features of an Fe(II) HS compound. On lowering the temperature, the compound changes spin state from high spin to low spin near 180 K, as is well documented by the Mössbauer spectra as a function of temperature, shown on the right-hand side of Figure 7.<sup>11,12</sup>

This kind of spin state switching is also possible by irradiation with light.<sup>11</sup> In view of the promising potential for practical application in devices,<sup>11</sup> both phenomena, thermal- and light-induced spin crossover, have been explored extensively in recent years by many research groups.

**Study of magnetotactic bacteria.** *Aquaspirillum magnetotacticum*, a magnetotactic bacterium living in the oceans, behaves as a biomagnetic compass and follows the weak geomagnetic field due to the presence of  $\text{Fe}_3\text{O}_4$  magnetic nanoparticles (40–120 nm) of hexagonal and cubic shapes in their bodies [Figure 8(a)]. The Mössbauer spectrum, recorded at 200 K, reveals two magnetic sextets typical of  $\text{Fe}_3\text{O}_4$ , an inverse spinel [Figure 8(b)]. The signals noted in the middle of the spectrum refer to Fe(III)-HS (B)

and Fe(II)-HS (C), which are assumed to serve as a reservoir for the formation of the magnetic particles.<sup>13</sup>

**Identification of iron–sulfur clusters in pharmacological relevant iron proteins.** One of the major successes of applications of Mössbauer spectroscopy in biological chemistry was the identification of the electronic states of polynuclear iron sulfur centres.<sup>14,15</sup> Very recently, Mössbauer spectroscopy has been used to identify an unusual 4Fe–4S-centre in the LytB-protein, also called IspH. This protein is crucial for the biosynthesis of

isoprenoids in many bacteria and in the malaria parasite *Plasmodium falciparum*. In these pathogens, isoprenoid synthesis occurs according to the methylerythritol phosphate (MEP) pathway, an alternative to the mevalonate pathway in higher organisms and humans.<sup>16</sup> Therefore, the MEP pathway is a valuable target for the development of new antimicrobial agents, as it is essential for microorganisms and absent in humans. Figure 9 shows how the Mössbauer spectrum of the LytB protein changes after the docking of its substrate and after binding of inhibiting substrate analogues which are promising molecules for future antibiotics and antiparasitic drugs.

**Corrosion studies.** Different oxides and oxyhydroxides of iron are known as corrosion products, which may be formed by corrosion processes in steel, metallic iron and iron containing alloys under different conditions. These corrosion products can be distinguished by  $^{57}\text{Fe}$  Mössbauer spectroscopy, even in the form of highly dispersed particles ( $>ca$  10 nm), where powder X-ray diffraction measurements are no longer applicable. Figure 10 shows the Mössbauer spectra of the most often occurring corrosion products. The spectra on the left were recorded at room temperature and identify the iron compounds

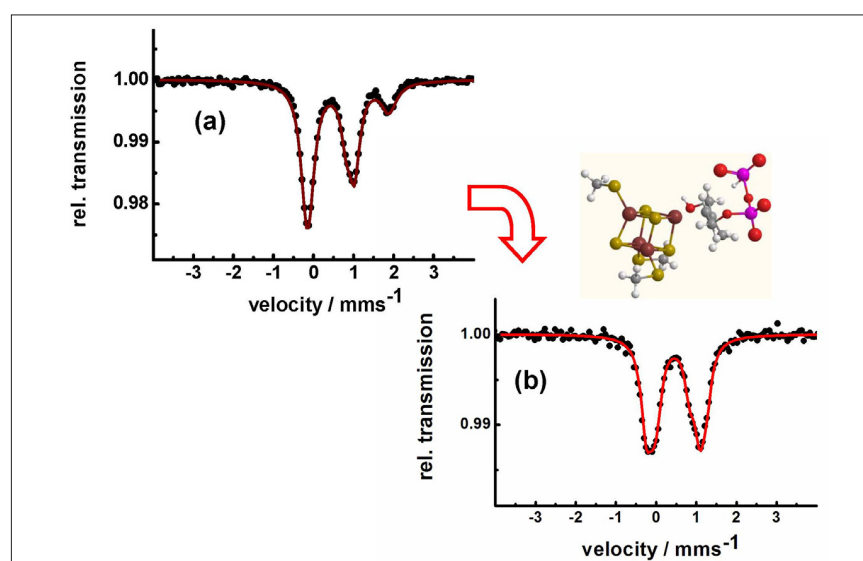


**Figure 9.** LytB (IspH) catalyses the last step of the methylerythritol phosphate pathway. Mössbauer spectroscopy shows that the substrate-free [4Fe-4S] cluster has a unique fourth iron site with parameters typical for tetrahedrally coordinated ferrous high-spin iron (a). The change in the pattern of the Mössbauer spectrum obtained after substrate addition (b) shows that the substrate is coordinating to the unique fourth iron site of LytB.<sup>16</sup>

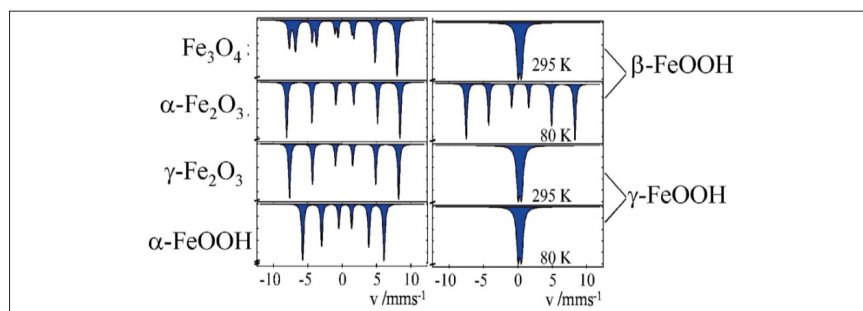


**Figure 10.**  $^{57}\text{Fe}$  Mössbauer spectra of various corrosion products of iron which may be formed under different conditions (reproduced from Reference 17 with permission).

through their magnetic behaviour. Spectra shown on the right are for the hydroxides  $\beta$ - and  $\gamma$ -FeOOH. The spectra recorded at room temperature are identical for the two compounds, but different when recorded at low temperature.

Such Mössbauer effect studies are carried out routinely to solve industrial corrosion problems. For instance, Figure 11 shows the Mössbauer spectrum of finely dispersed particles formed in the cooling system of a power plant. The spectrum is a superposition of the spectra of five different iron-containing species with concentrations given in the table.

### Mössbauer spectroscopy with a miniaturised portable spectrometer

Efforts to miniaturise Mössbauer instrumentation, which were started by Egbert Kankeleit in Darmstadt and continued by Göstar Klingelhöfer in Mainz, were driven by the desire to utilise Mössbauer spectroscopy for the exploration of the planet Mars. Space mission constraints of limited mass, volume and power

resulted in the miniaturised Mössbauer spectrometer MIMOS II<sup>4,18</sup> (Figure 12). It is set up in backscattering geometry, originally to eliminate the need for a complicated sample preparation mechanism on a Mars lander. Without the need to prepare powders or thin slices of samples for measurements and, together with its easy portability, MIMOS II allows for true non-destructive *in situ* analyses. Below we give a few examples of the new applications which are now possible.<sup>19</sup> The instrument is under continuous development. The latest version, MIMOS IIa, has the additional capability of acquiring X-ray fluorescence spectra.<sup>19,20</sup>

**Mars Exploration.** The Red Planet owes its colour to iron oxide pigments in the dust covering much of its surface and being dispersed in its atmosphere. The Martian mantle and crust are enriched in iron relative to Earth. It therefore seems a natural choice that NASA's twin Mars Exploration Rovers, Spirit and Opportunity, each have a Mössbauer spectrometer on board<sup>18</sup> (Figure 13). The rovers landed in January 2004. While communication with Spirit was

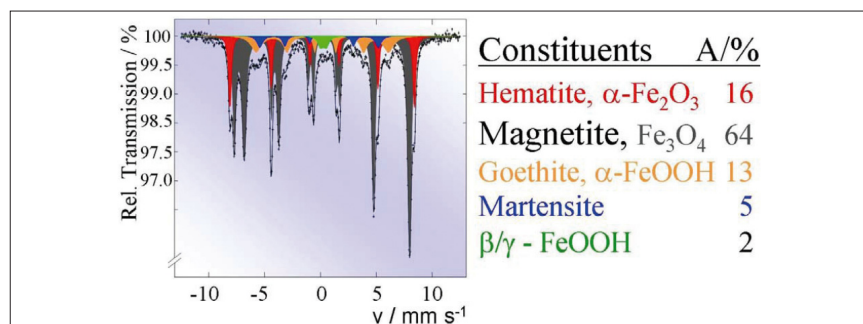


**Figure 11.** Routine Mössbauer analysis of finely dispersed corrosion particles formed in the cooling system of a power plant (reproduced from Reference 17 with permission).

lost in 2010, Opportunity is still actively exploring at the time of writing this article (July 2012). The primary scientific objectives of the mission are to explore sites on Mars where water may have been present at some point in the past, to assess the environmental conditions at that time and whether they would have been suitable for life.<sup>21</sup> Mössbauer spectroscopy addresses these objectives by characterising the distribution and speciation of iron in rocks and soil, which constrain rock types and crystallisation conditions of primary minerals as well as extent and pathways of alteration and weathering.<sup>22</sup>

The Mars rover Opportunity landed at Meridiani Planum where it encountered layered, sulfur-rich sedimentary rocks. While there is morphological evidence for water once even pooling at the surface, the best mineralogical evidence for water percolating through these rocks in the past is the identification by Mössbauer spectroscopy of the ferric sulfate hydroxide mineral jarosite.<sup>23</sup> The sedimentary rocks at Meridiani Planum contain 2wt% water from jarosite alone. Jarosite precipitates at a pH < 3.5 and, therefore, the water percolating the rock must have been acidic at the time of jarosite formation. While some microorganisms on Earth have adapted to low pH conditions, they challenge prebiotic chemical reactions which might have played a role in the origin of life on Earth.<sup>24</sup>

The Mars rover Spirit landed in Gusev Crater on the opposite side of the planet. Much of the crater floor is covered by a lava flow showing only very limited signs of aqueous alteration.<sup>25</sup> The older formations of the Columbia Hills protrude through that lava flow and reveal geochemical and mineralogical evidence for hydrothermal activity. Mössbauer spectra of one of the rocks investigated by Spirit in the Columbia Hills revealed a Ca-poor, Mg- and Fe-rich carbonate component that makes up 16 wt% to 34 wt% of the rock.<sup>26</sup> The chemical composition of the carbonate matches those identified from orbit at Nili Fossae, more than 6000 km distant from Gusev Crater and the carbonate globules in the Martian meteorite ALH84001. Nili Fossae, ALH84001 and the Columbia Hills date from the same epoch in Mars history



**Figure 12.** The sensorhead of the miniaturised Mössbauer spectrometer, MIMOS II, contains the drive unit, the Mössbauer source and the detectors and amplification electronics (adapted with permission from Reference 8).

and, therefore, imply that conditions were favourable for the formation of carbonates on a global scale at that time. The high carbonate concentration in the Columbia Hills rock is consistent with models of a warmer and wetter early Mars with CO<sub>2</sub> as a greenhouse gas that was subsequently, at least partially sequestered in carbonate minerals. Carbonates generally form in water at near-neutral pH, suggesting habitable environmental conditions during the time of formation.

**Geological field-work.** MIMOS II is well-suited for *in situ* analyses during geological field-work. Mixed-valent green rust minerals, for example, play an important role in redox reactions in anoxic groundwater and soil horizons. They are very oxygen-sensitive and, therefore, difficult to study in the laboratory. Feder *et al.* investigated changes in the oxidation state of the green rust mineral fougérite *in situ* in a gleysol as a function of time and depth.<sup>27</sup> The generalised formula of fougérite can be written  $[\text{Fe}^{2+}_{1-x}\text{Mg}_x\text{Fe}^{3+}_x(\text{OH})_{2+2g}]^{x+}[\text{xA}, \text{mH}_2\text{O}]^{-}$ , where  $x$  is the ratio  $\text{Fe}^{3+}/\text{Fe}_{\text{tot}}$  and A is the intercalated anion. To be able to measure repeatedly at the same depth but throughout the year during different seasons, a MIMOS II instrument was mounted into a Plexiglas tube.<sup>28</sup> The Plexiglas tube was lowered into a borehole into the gleysol at the

field site in Fougères, France, permitting investigations to a depth of about one metre. The variations that were observed by Mössbauer spectroscopy in the ratio  $x$ , as well as mineralogical changes, could be explained by seasonal fluctuations of

the water table.<sup>27</sup> The ratio  $x$  was approximately  $\frac{2}{3}$  in the upper soil horizons studied and  $\frac{1}{3}$  in the lower soil horizons. When the water table fell during summer, leading to aerobic conditions in the upper part of the soil, fougérite was completely oxidised to the ferric oxyhydroxide lepidocrocite ( $\gamma\text{-FeOOH}$ ). The supply of fresh organic matter and a rising water table during autumn reinstated anoxic conditions. Reduction and dissolution of lepidocrocite released  $\text{Fe}^{2+}$  into solution, accompanied by a soil colour change from ochre to blue and precipitation of fougérite.

**Art and archaeological artefacts.** When unique pieces of art or archaeological artefacts have to be investigated for conservational reasons, for example, it is self-evident that even removing tiny amounts of sample from these objects is not desirable. Whenever possible, non-destructive techniques should be favoured. In some cases, objects cannot be taken to the laboratory for analyses or transport may be too risky.<sup>29</sup> A portable Mössbauer spectrometer allows for the non-destructive *in situ* analysis

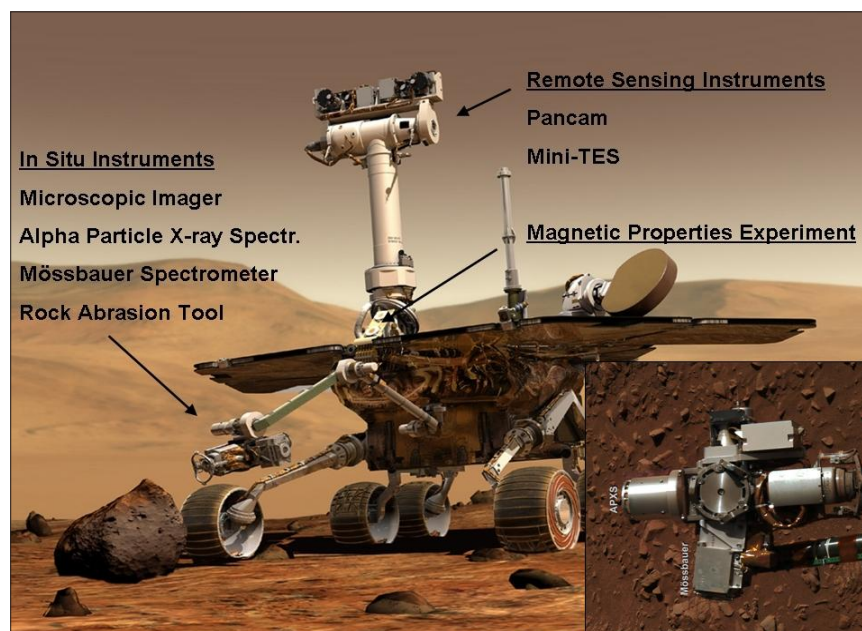


**Figure 13.** Artist's impression of the Athena payload of the two NASA Mars Exploration Rovers, Spirit and Opportunity. Inset is an image of the instruments on the robotic arm obtained with Spirit's Pancam on sol 287 of her mission: The Alpha Particle X-ray Spectrometer (pointing to the left), the Mössbauer spectrometer (down), the Rock Abrasion Tool (right) and the Microscopic Imager (up). A sol is a day on Mars, slightly longer than 24 h. The two Panoramic Camera (Pancam) "eyes" on top of the mast are at a height of approximately 1.5 m. Images: NASA/JPL/Cornell.

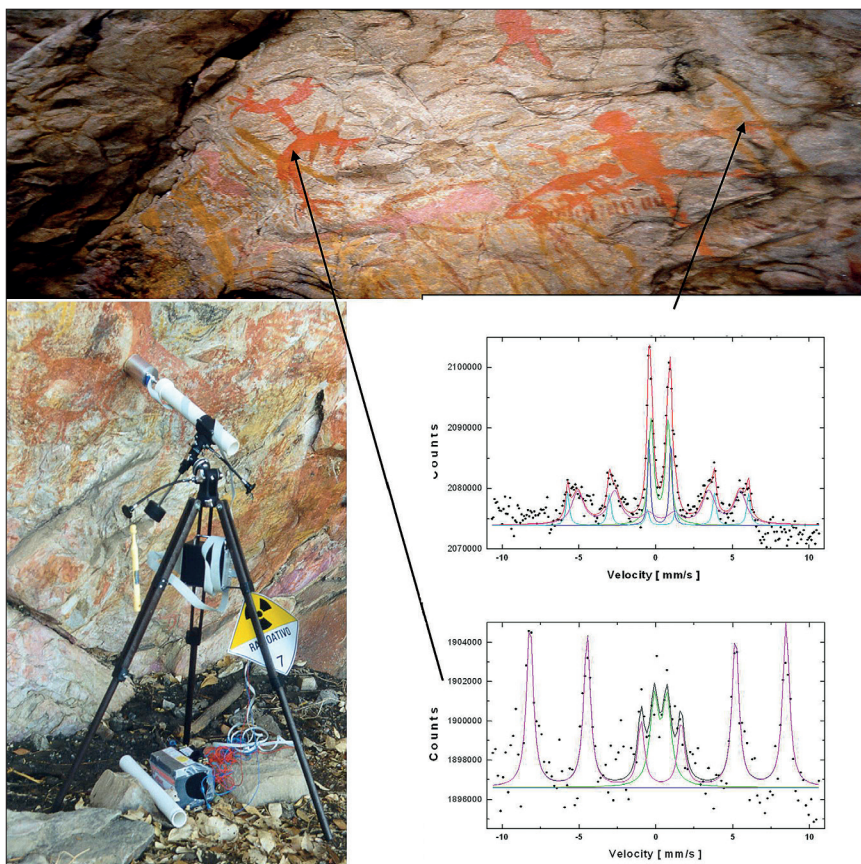


**Figure 14.** Non-destructive analysis with MIMOS of ancient rock paintings near Belo Horizonte, Minas Gerais, Brazil. MIMOS is mounted on a tripod and pointed at the different colours to be investigated. The spectra shown were recorded from a red area and an ochre area.

of such objects. One example is the characterization of iron oxide pigments used for different colours in rock paintings near Belo Horizonte, Minas Gerais, Brazil<sup>30</sup> (Figure 14). A MIMOS instrument was mounted on a tripod and pointed at different areas of colour within the paintings. Mössbauer spectra of red colour are dominated by a hematite ( $\alpha\text{-Fe}_2\text{O}_3$ ) signature; yellowish colours show goethite ( $\alpha\text{-FeOOH}$ ) signatures.

### Mössbauer spectroscopy with synchrotron radiation

Mössbauer spectroscopy with synchrotron radiation has an advantage over the conventional technique because the synchrotron beam can be conveniently focused. The high brilliance and the extremely collimated beam thus allow the measuring of samples with diameters of a few micrometres in less than one

hour. Also, experiments on interfaces and surfaces with sub-monolayer coverage of Mössbauer-active  $^{57}\text{Fe}$  atoms are, nowadays, almost routine at third generation synchrotron sources such as ESRF (Grenoble, France), APS (Argonne National Laboratory, USA), SPRING-8 (Hyōgu Prefecture, Japan) and PETRA III (DESY, Germany).

### Nuclear forward scattering

Coherent nuclear resonant forward scattering (NFS) can be regarded as Mössbauer spectroscopy in the time domain.<sup>31,32</sup> A pulse of monochromatised synchrotron radiation is used to excite the  $^{57}\text{Fe}$  nuclei in the sample. Due to the long lifetime (141 ns) of the 14.4 keV excited state the radiation is re-emitted with a delay which is sufficient to discriminate it from the promptly scattered quanta by time-gated detectors (Figure 15). The time dependence of the coherently forward scattered radiation is determined by the hyperfine parameters (isomer shift, electric field gradient and hyperfine field) and the dynamics of the iron. NFS allows the direct determination of these parameters including the Lamb-Mössbauer factor.<sup>33,34</sup>

### Nuclear inelastic scattering

Nuclear inelastic scattering (NIS) of synchrotron radiation can be regarded as an extension of the conventional, energy-resolved Mössbauer spectroscopy to energies of phonons or molecular vibrations.<sup>35,36</sup> Therefore, this technique is also called nuclear resonance vibrational spectroscopy (NRVS). In contrast to a NFS-experiment, the energy of the incoming radiation  $E_i$  is varied within an interval of up to  $\pm 100$  meV around the resonance energy,  $E = 14.4$  keV, of the Mössbauer nucleus (see Figure 16 for a typical spectrum). In a NIS experiment, the absorption probability is measured as a function of the energy difference  $E - E_i$ . An advantage of the NIS technique, when compared to other vibrational spectroscopies, is that it is a site-selective method, which solely

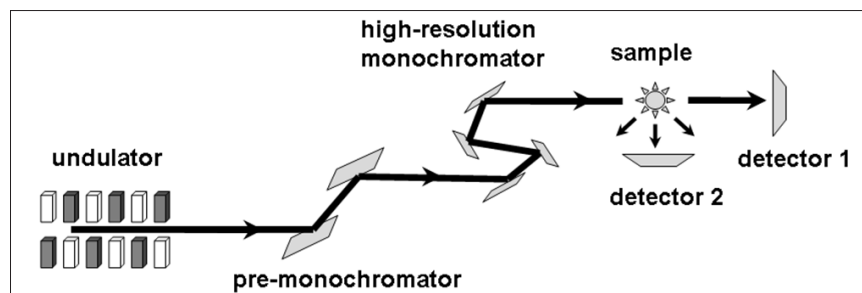


**Figure 15.** Set-up for Nuclear Forward Scattering (NFS) and Nuclear Inelastic Scattering (NIS). For NFS coherent scattering is detected by detector #2 and for NIS incoherent scattering is detected by detector #1 (adapted with permission from Reference 8).

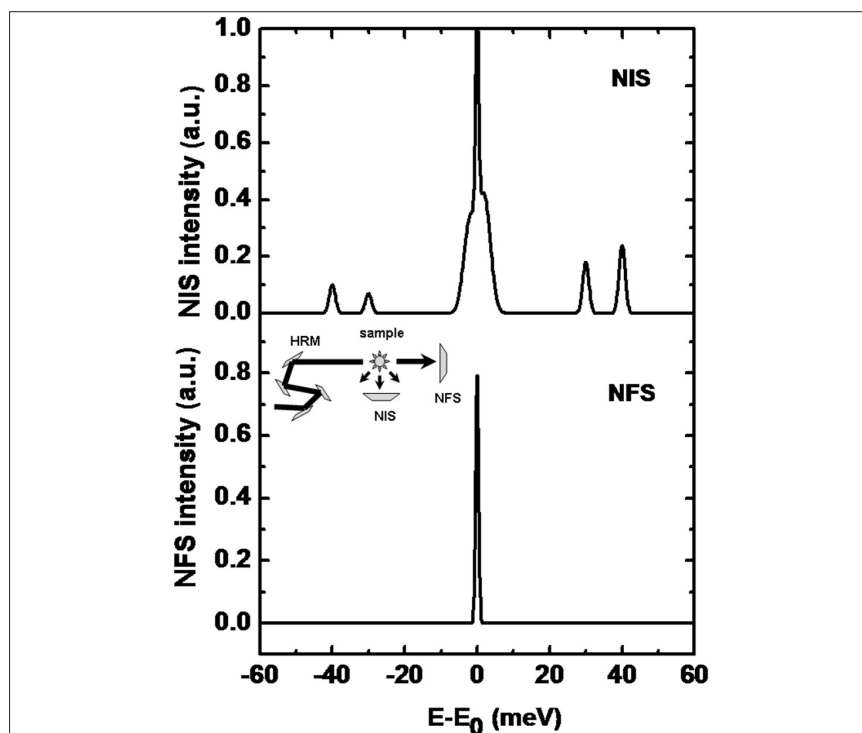


**Figure 16.** (Top) A sketch of a typical NIS spectrum. A high-resolution monochromator (HRM, see inset) is tuned around the nuclear resonance. The scattered intensity in forward direction (NFS) and perpendicular to the incoming beam (NIS) is monitored as a function of energy relative to  $E_\gamma$  (14.4 keV in case of  $^{57}\text{Fe}$ ). Around  $E=E_\gamma$ , the elastic peak is overlaying the corresponding energy sidebands which are caused by phonon creation ( $E>E_\gamma$ ) and phonon annihilation ( $E<E_\gamma$ ). (Bottom) The spectrum shows the intensity of the forward scattered radiation which is called the instrumental function.

detects the dynamics of the active site iron: the intensity of individual peaks in a spectrum is roughly proportional to the mean-square displacement of the Mössbauer nucleus arising from the corresponding molecular vibration. Different from infrared or Raman spectroscopy, NIS spectra depend solely on mechanical properties, i.e. the eigenfrequencies and eigenvectors of the vibrations, but not on electrical properties such as the polarisability of the molecule.<sup>37</sup> For this reason, NIS can be calculated by theoretical methods with good reliability.

**Surface science applications: When is a solid a solid?** Stankov *et al.* have followed with NIS measurements the change of the phonon density of states (DOS) of body-centred cubic (bcc) iron starting with epitaxial monolayers.<sup>38</sup> The bulk-like DOS was reached after depositing ten monolayers of  $^{57}\text{Fe}$  on the surface of a tungsten (100) surface (Figure 17). Below film thicknesses of ten monolayer deviations result from atomic vibrations of the single atomic layers at the two boundaries of the film, while the atoms inside the film vibrate almost bulk-like.

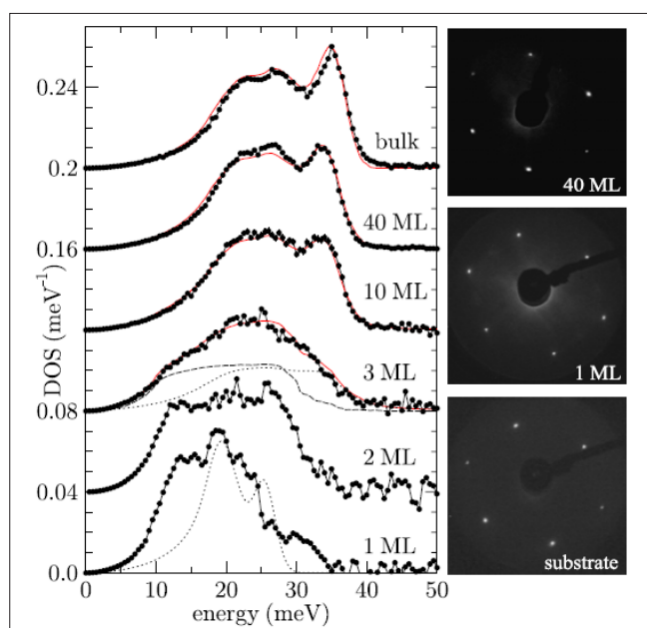


**Figure 17.** Iron density of phonon states (DOS) of single-crystalline Fe films on W(110) for thicknesses ranging from a monolayer (ML) to a 40 ML thick film. The solid line in the upper graph represents the density of phonon states of polycrystalline bulk  $\alpha$ -iron, i.e., the ambient temperature bcc phase of iron. (Adapted with permission from Reference 38. Copyright 2007 by the American Physical Society.)

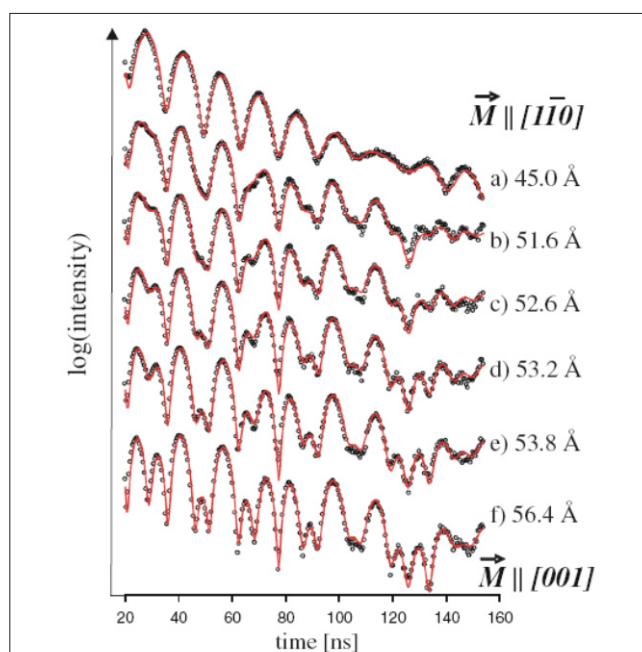


**Figure 18.** NFS spectra accumulated during continuous Fe evaporation labelled with the corresponding Fe thicknesses. The theoretical analysis (red curve) shows the indicated spin-reorientation of the bcc iron magnetisation  $\vec{M}$ . (Adapted with permission from Reference 39. Copyright 2010 by the American Physical Society.)

NFS has been used extensively to study the magnetic behaviour of iron monolayers as well as thin films. An example is the exploration of the magnetisation structure during the thickness-induced spin-reorientation transition (SRT) for a metallic iron film grown on a  $W(110)$  surface.<sup>39</sup> Figure 18 shows the NFS data accumulated during continuous iron evaporation with film thicknesses of 45 Å up to 56.4 Å. The experimental trace changes significantly, which could be interpreted as reorientation of the film magnetisation from being parallel to the  $[1\bar{1}0]$  axis in the case of a 45 Å film to the  $[001]$  direction of films with thicknesses larger than 56 Å.

**Application of NIS and NFS to high pressure research.** NIS has been successfully applied to measure the density of phonon states (DOS) in iron under high pressure up to 153 GPa by Wortmann and co-workers at the European Synchrotron Facility (ESRF) in Grenoble<sup>40</sup> and the Advanced Photon Source (APS) at Argonne.<sup>41</sup> From the measured DOS elastic and thermodynamic parameters of the high pressure hexagonal-closed packed iron phase including shear modulus, compressional and shear velocities, heat capacity, entropy, kinetic energy, zero point energy and Debye temperature, have been obtained. From the comparison with the PREM (primary reference earth model) seismic model, the authors concluded that the Earth's inner core has a mean atomic number equal to or higher than pure iron which is consistent with an iron nickel alloy. Recently, even a pressure-induced spin transition of ferrous iron from the high-spin to the intermediate-spin state at approximately 30 GPa in iron-containing perovskite, which is a major constituent of the earth's mantle, has been observed by NFS.<sup>42</sup>

**NIS on single crystals of molecular complexes.** In particular, the combination of NIS and quantum mechanical calculations (DFT) enables one to fully understand not only the electronic properties but also the dynamics of iron containing molecular complexes. As an example, orientation-dependent NIS spectra of an Fe(II) molecular crystal are given in Figure 19. Recently, the high- to

low-spin transition of Fe(II) complexes at high pressures has also been studied using this technique.<sup>43,44</sup>

**NIS enlightens binding of cardiovascular regulatory nitric oxide to haeme proteins.** Nitric oxide (NO), plays an essential role as a signal molecule for cardiovascular regulation. A transatlantic cooperation between German, US-American and ESRF scientists has recently investigated the binding mechanism of NO to the transporter haeme protein, nitrophorin, which occurs not only in the saliva of the blood-sucking Amazon river-based kissing bug, *Rhodnius prolixus*, but also in the bedbug, *Cimex lectularius*, found worldwide. It turned out that NIS could not only pin down haeme NO binding modes, but also possibly functionally relevant low-energy modes at energies down to  $10 \text{ cm}^{-1}$  (see Reference 46). Furthermore, indications have been found that protonation of the haeme carboxyls may modulate NO capture and release. These results are important with regard to a potential application of these types of NO carrier proteins as cardiovascular drugs. The NIS

data shown in Figure 20(a) have also been calculated using DFT methods coupled with molecular mechanics methods. The simulations not only identify Fe–NO binding modes [Figure 20(d)], but also functionally relevant low-energy modes.<sup>47</sup>

## Concluding remarks

In this article we have tried to showcase applications of Mössbauer spectroscopy from a broad variety of research fields. Of course, the examples presented by no means give a complete overview. New applications for conventional Mössbauer spectroscopy continue to be found. The miniaturised, portable MIMOS opens up many new possibilities of non-destructive, *in situ* investigations. The number of applications and demand for NFS and NIS grow at rapid speed and, therefore, the number of synchrotron facilities around the world with dedicated beamlines continues to increase. More than 50 years after the discovery of the Mössbauer effect, Mössbauer spectroscopy remains a technique with a growing number of applications.

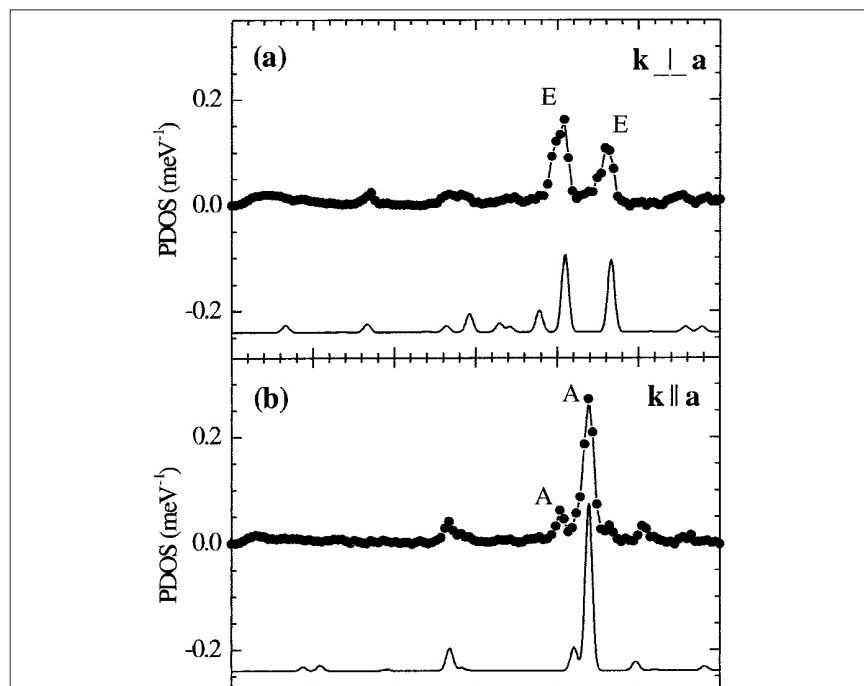


**Figure 19.** Orientation-dependent NIS spectra of an Fe(II) molecular crystal oriented with the crystallographic  $a$ -axis perpendicular (a) and parallel (b) to the direction of the synchrotron beam. The spectral features are due to molecular vibrations and very well reproduced by theoretical spectra calculated on the basis of DFT-calculations shown below. (Adapted with permission from Reference 45. Copyright 2001 by the American Physical Society.)

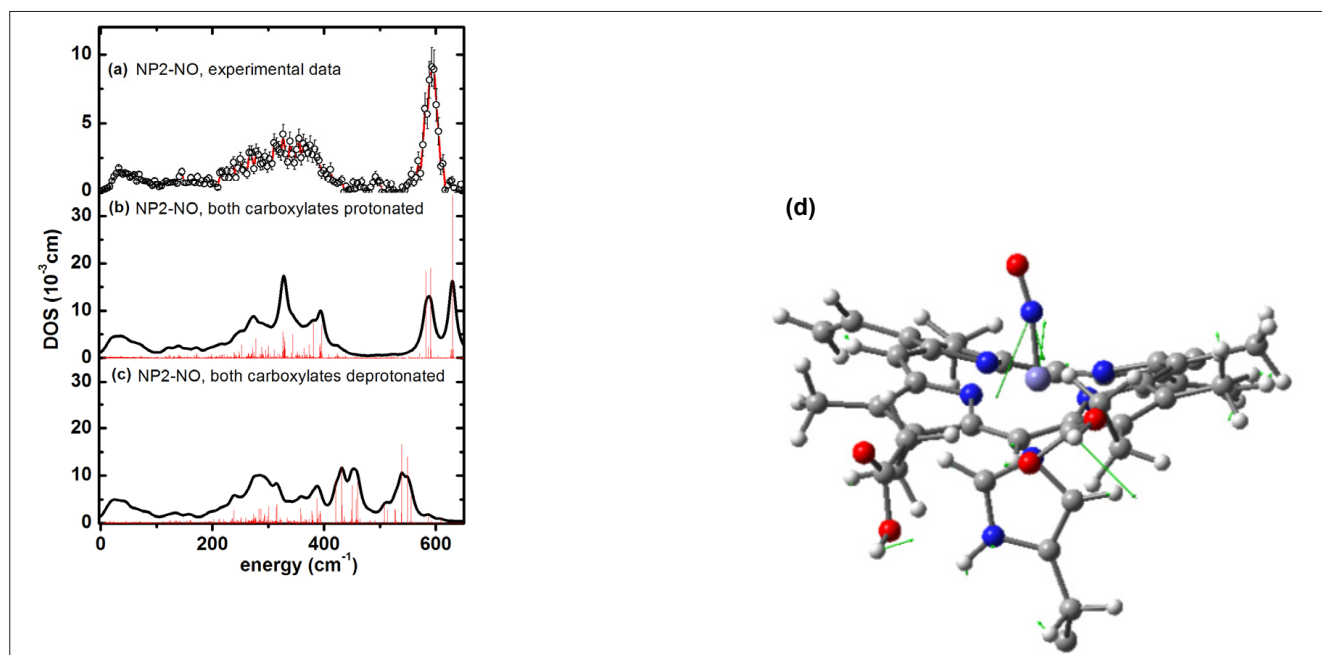


**Figure 20.** Iron vibrational density of states (DOS) for NP2-NO: (a) experimental data, (b) simulation with both haeme carboxylates protonated and (c) with both haeme carboxylates deprotonated (reprinted with permission from Reference 46. Copyright (2012) American Chemical Society). (d) Representation of a calculated normal mode of NP2-NO at  $630\text{ cm}^{-1}$  with the optimised haeme structure of NP2-NO used for calculating the NIS data shown. Only the parts of the molecules treated with DFT are displayed. The residual parts of the protein, which were taken into account by force field calculations, are not shown. The arrows describe atom movements of the protein mode with significant Fe-NO stretching character.<sup>47</sup>

## References

- R.L. Mössbauer, "Gammastrahlung in Ir191" ["Nuclear resonance absorption of gamma rays in Ir191"] *Z. Physik* **151**, 124 (1958).
- R.L. Mössbauer, "Kernresonanzabsorption von Gammastrahlung in Ir191", *Naturwissenschaften* **45**, 538 (1958). doi: 10.1007/BF00632050
- R.L. Mössbauer, *Z. Naturforsch.* **14a**, 211 (1959).
- G. Klingelhöfer, *The miniaturized spectrometer MIMOS II*, in: Reference 8.
- E. Gerdau, R. Rüffer, H. Winkler, W. Tolksdorf, C.P. Klages and J.P. Hannon, "Nuclear Bragg diffraction of synchrotron radiation in yttrium iron garnet", *Phys. Rev. Lett.* **54**, 835 (1985). doi: 10.1103/PhysRevLett.54.835
- N.N. Greenwood and T.C. Gibb, *Mössbauer Spectroscopy*. Chapman and Hall, London, UK (1971). doi: 10.1007/978-94-009-5697-1
- G.J. Long (Ed.), *Mössbauer Spectroscopy Applied to Inorganic Chemistry*, 1 (and subsequent volumes). Plenum Press, New York, USA (1984).
- P. Gütlisch, E. Bill and A.X. Trautwein, *Mössbauer Spectroscopy and Transition Metal Chemistry—Fundamentals and Applications*, Springer-Verlag, Heidelberg, Germany (2011).
- J.G. Stevens and V.E. Stevens, *Mössbauer Effect Data Index 1965–1975*. Adam Hilger London, UK.
- P. Gütlisch, A. Hauser and H. Spiering, "Thermal and optical switching of iron(II) complexes", *Angew. Chem. Int. Ed. Engl.* **33**, 2024 (1994). doi: 10.1002/anie.199420241
- P. Gütlisch and H.A. Goodwin (Eds), *Spin Crossover in Transition Metal Compounds, I, II and III, Topics in Current Chemistry Series*, Vols 233, 234 and 235. Springer-Verlag, Heidelberg, Germany (2004).
- I. Dezsi, B. Molnar, T. Tamoczi and K. Tompa, "On the magnetic behaviour of iron(II)-bis-(1,10 phenantroline)-thiocyanate between  $-190^\circ$  and  $30^\circ\text{ C}$ ", *J. Inorg. Nucl. Chem.* **29**, 2486 (1967).
- R.B. Frankel, G.C. Papaefthymiou, R.P. Blakemore and W. O'Brien, " $\text{Fe}_3\text{O}_4$  precipitation in agnetotactic bacteria", *Biochim. Biophys. Acta* **763**, 147 (1983). doi: 10.1016/0167-4889(83)90038-1
- H. Beinert, R.H. Holm and E. Münk, "Iron-sulfur clusters: Nature's modular,

## Silicon Drift Detector

### SUPER SDD

**XRF Experimenter's Kit**

**OEM Components**

**Complete X-Ray Spectrometer**

**XRF System**

**OEM's #1 Choice for XRF**

**www.amptek.com**

**FASTLINK / ENTER 010 FOR FURTHER INFORMATION**